

Selective Bond Dissociation and Rearrangement with Optimally Tailored, Strong-Field Laser Pulses

Robert J. Levis,^{1*} Getahun M. Menkir,¹ Herschel Rabitz²

We used strong-field laser pulses that were tailored with closed-loop optimal control to govern specified chemical dissociation and reactivity channels in a series of organic molecules. Selective cleavage and rearrangement of chemical bonds having dissociation energies up to approximately 100 kilocalories per mole (about 4 electron volts) are reported for polyatomic molecules, including $(\text{CH}_3)_2\text{CO}$ (acetone), CH_3COCF_3 (trifluoroacetone), and $\text{C}_6\text{H}_5\text{COCH}_3$ (acetophenone). Control over the formation of CH_3CO from $(\text{CH}_3)_2\text{CO}$, CF_3 (or CH_3) from CH_3COCF_3 , and $\text{C}_6\text{H}_5\text{CH}_3$ (toluene) from $\text{C}_6\text{H}_5\text{COCH}_3$ was observed with high selectivity. Strong-field control appears to have generic applicability for manipulating molecular reactivity because the tailored intense laser fields (about 10^{13} watts per square centimeter) can dynamically Stark shift many excited states into resonance, and consequently, the method is not confined by resonant spectral restrictions found in the perturbative (weak-field) regime.

that arrays of molecular devices can be produced by design with the use of external electrical means and without a need for actual control at the nanometer scale. Discretionary modification allowed the definition of useful electronic elements from a random mixture. Though we have applied this solution to solve the problem of variation inherent to carbon nanotubes, one could imagine generating similar results using mixtures of carefully chosen molecules. In that more general sense, the possibilities for active circuitry have yet to be explored.

References and Notes

- H. Dai, E. W. Wong, C. M. Lieber, *Science* **272**, 523 (1996).
- J. E. Fischer *et al.*, *Phys. Rev. B* **55**, R4921 (1997).
- S. J. Tans, A. R. M. Verschueren, C. Dekker, *Nature* **393**, 49 (1998).
- R. Martel, T. Schmidt, H. R. Shea, T. Hertel, Ph. Avouris, *Appl. Phys. Lett.* **73**, 2447 (1998).
- L. Chico, V. H. Crespi, L. X. Benedict, S. G. Louie, M. L. Cohen, *Phys. Rev. Lett.* **76**, 971 (1996).
- R. Saito, G. Dresselhaus, M. S. Dresselhaus, *Phys. Rev. B* **53**, 2044 (1996).
- MWNTs for this study were provided by W. deHeer and were grown by standard arc techniques. SWNTs were provided by R. Smalley and were grown by metal-catalyzed laser ablation. Both types of nanotubes were dispersed in dichloroethane and purified solely by centrifugation.
- P. G. Collins, M. Arnold, M. Hersam, R. Martel, Ph. Avouris, *Phys. Rev. Lett.* **86**, 3128 (2001).
- R. Saito, G. Dresselhaus, M. S. Dresselhaus, *J. Appl. Phys.* **73**, 494 (1993).
- A. Bachtold, *et al.*, *Nature* **397**, 673 (1999).
- S. Frank, P. Poncharal, Z. L. Wang, W. A. de Heer, *Science* **280**, 1744 (1998).
- C. Schöenenberger, A. Bachtold, C. Strunk, J.-P. Salvetat, L. Forro, *Appl. Phys. A* **69**, 283 (1999).
- S. Iijima, *Nature* **354**, 56 (1991).
- C.-H. Kiang, M. Endo, P. M. Ajayan, G. Dresselhaus, M. S. Dresselhaus, *Phys. Rev. Lett.* **81**, 1869 (1998).
- The use of high-voltage pulses to break shells leads to some rearrangement of trapped charges on the underlying SiO_2 substrate. To simplify the comparison among shells, we centered each curve in Fig. 2B near $V_g = 0$.
- J. W. Mintmire, B. I. Dunlap, C. T. White, *Phys. Rev. Lett.* **68**, 631 (1992).
- R. Saito, M. Fujita, G. Dresselhaus, M. S. Dresselhaus, *Phys. Rev. B* **46**, 1804 (1992).
- High-bias I - V curves must be acquired in high vacuum to suppress destructive oxidation. Between each curve, the MWNT was exposed to air in order to remove single carbon shells in a controlled manner. Four- and two-probe measurements are periodically compared to monitor the contact resistance R_c to each nanotube. The data shown here are for samples exhibiting constant R_c of a few kilohms throughout the series of measurements. Samples with high R_c tend to fail at the contact, as opposed to the shell-by-shell mechanism described here.
- Z. Yao, C. L. Kane, C. Dekker, *Phys. Rev. Lett.* **84**, 2941 (2000).
- For example, see H. Stahl, J. Appenzeller, R. Martel, Ph. Avouris, B. Lengeler, *Phys. Rev. Lett.* **85**, 5186 (2000).
- The remaining 10% form open circuits before we can achieve complete switching. Imaging these samples typically reveals large contaminant particles or multiprobe crossings, which likely result in weak, dissipative links.
- We thank R. Martel for valuable discussions, K. J. Chan for assistance with lithography, and B. Ek for expert technical assistance. M.A. acknowledges the support of an IBM summer internship.

4 January 2001; accepted 5 March 2001

The control of organic chemistry with optical fields has been a long-sought-after goal. This objective goes beyond traditional photochemistry, where variation in the product distribution is obtained by tuning a monochromatic radiation source to excited states of a precursor molecule. Here, we focus on whether a suitably tailored laser pulse can guide a distribution of products to a specific channel, characterized by dissociation or rearrangement, as illustrated in Fig. 1. Successful control in this context implies cooperative interaction between a (perhaps complex) time-dependent electric field of the laser pulse and the precursor molecule's dynamics to alter the product distribution in a desirable and variable manner. The objective is to maximize the yield of a specified product by means of a suitable closed-loop laboratory learning procedure that determines the optimal laser pulse. The capability of controlling reactivity, especially of organic species, by this means could have implications in diverse industrial and biological or medicinal settings. For example, microelectronic lithography, the fabrication of gene chips, and photodynamic therapy could all benefit from highly controllable photochemistry.

Since the introduction of the concept of teaching lasers to control photodynamics with closed-loop methods (1), the process has been used for optimization of laser-induced fluorescence (2), stimulated Raman emission from molecules (3), high harmonic generation (4), ultrafast semiconductor switching

(5), and management of pulse propagation through nonlinear media (6). The first implementation of this scheme for dissociating bonds was demonstrated in groundbreaking work on organometallic systems (7) and has since been demonstrated in the cleavage of weakly bound cluster species (8). The control of organic reactivity, where bond strengths exceed ~ 50 kcal/mol, remains an open and important area of optical control research.

We demonstrate a potentially universal, ultrafast laser excitation procedure to achieve control over molecular reactivity. This procedure is based on closed-loop learning of optimally shaped, strong-field, near-infrared pulses (centered around 800 nm) guided just by the desired product. A strong-field laser pulse ($\sim 10^{13}$ W cm^{-2}) implies that the associated electric field magnitude is on the order of the valence electron's binding energy in the molecule. This magnitude is a critical enabling feature for broad-scale application upon consideration of the bandwidth required for the effective control of chemical reactions. Weak-field, continuous wave pulses must be precisely tuned to a molecular resonance for coupling; Fig. 2A represents such an excitation scheme for most conventional photochemical reactions. Ultrafast laser systems allow ~ 0.1 eV of bandwidth for a 25-fs pulse (for example, 775 to 825 nm for a near-infrared pulse). The relatively small bandwidth around the laser carrier frequency limits control in the weak-field case (Fig. 2B). However, with strong-field pulses, the nominal eigenstates of the molecule can be placed into resonance through a combination of Stark shifting (up to ~ 10 eV in our experiment) (9) and multiphoton excitation (10 to 50 photons using the Ti:sapphire laser cen-

¹Department of Chemistry, Wayne State University, Detroit, MI 48202, USA. ²Department of Chemistry, Princeton University, Princeton, NJ 08540, USA.

*To whom correspondence should be addressed.

REPORTS

tered at 800 nm) (10, 11) (Fig. 2C). The latter two strong-field excitation mechanisms effectively remove bandwidth restrictions. The linear modulation of the strong field provided by the pulse shaper leads to control of the ensuing highly nonlinear molecular dynamics response. Transitions may be moved in and out of resonance as dictated by the pulse structure to optimally achieve the chemical objective. An example of three time-dependent electric fields (shaped laser pulses) producing different products is shown in Fig. 2D.

A shaped laser pulse has an electric field with possibly complex time-dependent structure, and suitable manipulation of this structure has the potential to guide a molecule to a specified product. The shaped pulses are produced by spatial light modulation of both the phase and amplitude of the component frequencies in an ultrafast transform-limited pulse (12). It is possible to rapidly synthesize a large number of pulses, each of which will interact with the molecule in a different nontrivial manner, giving rise to a combinatorial photochemistry (13). We used time-of-flight (TOF) mass spectrometry to detect selective bond cleavage or chemical rearrangement after application of each shaped strong-field pulse. The concept is demonstrated here with acetone, trifluoroacetone, and acetophenone.

For strong-field manipulation of polyatomic molecules, the ultimate effect of a laser pulse cannot be calculated by any method at present. However, the molecule rapidly “solves” the Schrödinger equation governing its dynamics in real time when exposed to the laser field (1, 14). Thus, these experiments use the molecule under control as an “analog computer” to guide the shaping of subsequent laser pulses to better achieve the objective. Previous strong-field investigations with unshaped pulses applied to organic molecules have revealed a distribution of products ranging from intact ionization to substantial decomposition (15). The learning algorithm strives to tailor the optimal electric field to synthesize a specific chemical product in competition with the other possible outcomes

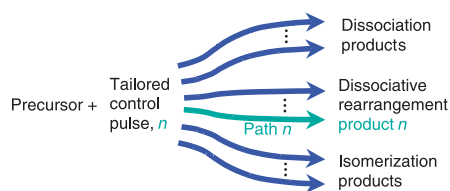


Fig. 1. A schematic of control over chemical reaction pathways with tailored, strong-field laser pulses. By using feedback from the observed reaction products, a learning algorithm can guide an evolving laser pulse shaper to achieve the desired product as best as possible. The experiments presented here focused on dissociation and dissociative rearrangement reactions for ketone molecules.

(Fig. 1). Nonrobust fields are immediately discriminated against in the closed-loop approach (16).

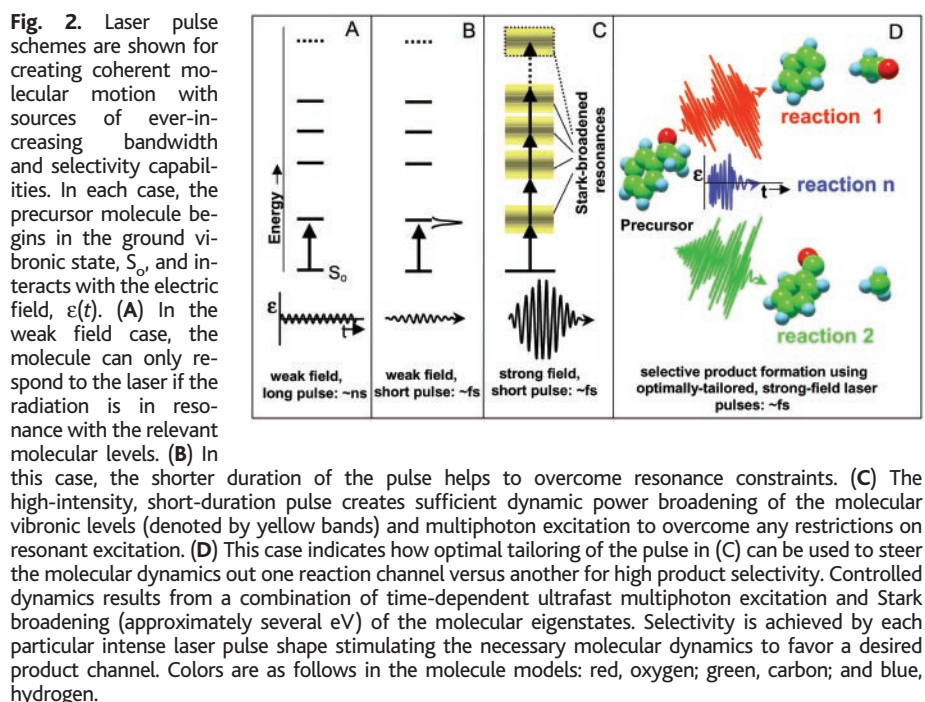
The time-dependent electric field was produced by first dispersing the frequencies comprising the short pulse with a grating, thus transforming the pulse from the time domain into the frequency domain. The light was collimated with a cylindrical lens to produce a ribbon of light (the Fourier plane) 13 mm wide, where the frequencies may be addressed spatially (17). In our experiment, the radiation was discretized into 128 frequency bands, or components, by using a liquid crystal spatial light modulator (SLM). Each of the 128 elements in the SLM is 100 μm wide, with 3 μm of dead space between pixels. The relative phase and amplitude of each component can be altered independently with a pair of SLMs followed by a polarizer. After recombining the modulated frequency components with a second lens/grating pair, one obtains a time-dependent electric field that is unique to the phase and amplitude masks employed.

We can efficiently determine the optimal time-dependent electric field by using a genetic algorithm (18) to control the spatial light modulation. The algorithm creates and manages the 256 voltages (the genome) that determine the phase and amplitude of the component frequencies that control, in turn, the time-dependent structure of the laser pulses. A population of 40 distinct laser pulses (genomes) was propagated to determine the optimal pulse for a desired reaction. The laser pulses are randomly generated on the first cycle around the loop, with the restriction in our experiment that groups of 16 neighboring

pixels are tied together to effectively make a genome with 16 variable sites. Each of these sites specifies a retardance that controls the phase and amplitude of the component frequencies. This process creates a search space of 360^{16} ($\sim 10^{41}$) possible control fields given 1° resolution in 360° for the phase delay. Searching through this phase space may seem to be an insurmountable problem, but efficient methods have been developed and many distinct fields likely exist that give good quality control results (19). In subsequent generations, fields are selected for propagation using proportional selection, and new fields are generated by random crossover and mutation with a rate of 6% per field member.

The modulated laser pulses were focused to a 100- μm -diameter spot to interact with the molecules at 300 K and 10^{-6} torr. Spatial nonuniformity in the focal volume can produce localized laser intensity variations, but the learning algorithm will work to best overcome these differences (20). The intensity variations were further accounted for by using a 500- μm -diameter extraction aperture in the ion optics to select products from the most intense portion of the laser beam. The resulting TOF spectra were measured and signal-averaged eight times for each trial laser pulse shape, requiring ~ 40 s to evolve a generation with a 10-Hz repetition rate laser. For these experiments, we found that acceptable convergence rates were obtained when the most fit member was cloned twice in the succeeding generation.

We investigated whether the overall algorithm could determine a suitable control field from both the large search space and nonlinear excitation scheme by beginning with a



case where a viable solution was known in advance. A series of reference experiments (21) revealed that intense, transform-limited pulses (5×10^{13} W cm $^{-2}$, 800 nm, 60 fs) produced a substantial quantity of the CH_3CO^+ ion from acetone. The evolution of the strong-field mass spectrum is displayed in Fig. 3A as a function of generation when the goal was optimization of the peak at a mass-to-charge ratio of 43 atomic mass units (amu) (CH_3CO^+). Although the CH_3CO^+ ion was almost unobservable in the first generation, the signal intensity was sufficient for the algorithm to begin optimization. The experiment produced exponential growth in the early generations, as seen in Fig. 3B. Analysis of the SLM mask revealed that the algorithm was indeed selecting a nearly transform-limited pulse to produce the CH_3CO^+ . The yield increased approximately an order of magnitude by the fifth generation where the enhancement was saturated. In subsequent generations, the signal varied because of changes in the control field introduced by mutation and crossover. This experiment demonstrated that the closed-loop learning process with a genetic algorithm is an efficient method for controlling photodissociation and ionization yields when strong-field excitation is employed. Furthermore, this experiment showed that the mass spectrum of a molecule can be dramatically altered with tailored excitation pulse shapes. This capacity for multidimensional analysis could be of considerable value for determining the identity of complex molecules, because widely varying mass spectral

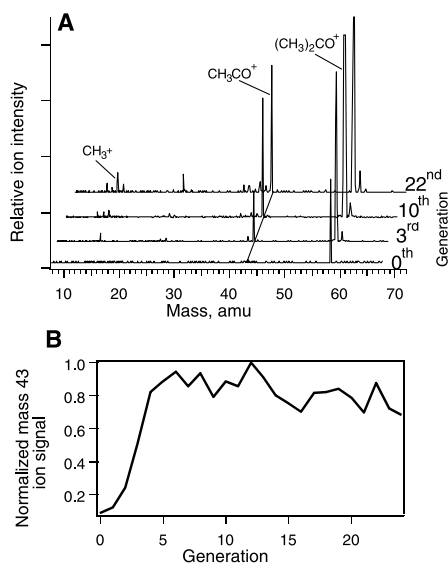


Fig. 3. (A) A representative mass spectra of acetone for the initial 0th, 3rd, 10th, and 22nd generations when maximization of the CH_3CO^+ ion from acetone is specified. (B) The CH_3CO^+ signal as a function of generation of the genetic algorithm. In (B) and the following plots of this type in Figs. 4 and 5, the average signal for the members of the population at each generation is shown.

ion distributions (each with different information content) can be obtained as a function of pulse shape. Dissociation need not be a distinct step before ionization occurs. In general, the strong-field pulse will prepare the optimal excited wave function to evolve into the desired products for detection.

It is convenient to define two classes of mechanism for the control of strong-field photochemistry: trivial control and nontrivial control. Trivial control refers to simple intensity or pulse duration effects leading to the observed photochemistry; pulse-shaping technology is not necessary when trivial control is satisfactory. Increasing intensity ultimately leads to increasing the dissociative ionization yield in the strong-field mass spectrum (22). Furthermore, increasing the laser pulse duration also alters the degree of dissociation observed in strong-field excitation. The intensity and pulse duration reference experiments for acetone (23) demonstrate that most of the control exerted arises from intensity effects. Cases exhibiting nontrivial control arise from the cooperative interaction of the laser pulse shape with an evolving molecular wave packet. For nontrivial control, the product distribution can be sensitive to the precise time-dependent structure in the pulse. In the strong-field regime, the dynamics could incorporate multiple electronic states in subtle ways to manipulate the dissociation or rearrangement to meet the posed objectives, as suggested by Fig. 2, C and D.

To determine whether the control process is trivial or nontrivial in any particular case, we

compared the absolute and relative yields for two different ions as a function of generation in the genetic algorithm to those obtained from the simple intensity and pulse duration reference experiments. Such a closed-loop experiment is shown in Fig. 4 for trifluoroacetone (CH_3COCF_3), where two different objectives are presented. Maximization of the ratio $\text{CF}_3^+/\text{CH}_3^+$ is shown in Fig. 4A, and maximization of the ratio $\text{CH}_3^+/\text{CF}_3^+$ is shown in Fig. 4B. The ion intensities are normalized to that obtained for the initial random pulses in generation zero, and the ratios are scaled to unity at generation zero. Initially, the absolute ion yields of CH_3^+ and CF_3^+ were within a factor of 2 in both experiments. In Fig. 4B, the optimal ratio is obtained on the 13th and again on the 21st generation, with the surrounding forays producing lesser yields. In the closed-loop experiment, the optimal genome was stored (for example, at the 13th generation) and was available for use at later times; thus, in this case, the largest reproducible ratio was ~ 2.2 . The trend during the maximization in each case is declining total ion signal. The reference experiments (21) for trifluoroacetone reveal no trend in the $\text{CF}_3^+/\text{CH}_3^+$ ratio as a function of laser intensity, which eliminated the possibility of trivial intensity control. Considering trivial pulse duration control, the reference experiments reveal that the $\text{CF}_3^+/\text{CH}_3^+$ ratio actually decreased with increasing pulse duration, which is opposite to the trend shown in Fig. 4A.

The degree of shaped-pulse control exerted in the case of trifluoroacetone could arise because of the widely different electronegativities available when fluorinated substituents are used. We therefore investigated acetophenone cleavage to determine whether control is possible in the case of hydrocarbon functional groups. The transform-limited, strong-field mass spectrum for acetophenone is shown in Fig. 5A, where several complementary pairs of ions in the transform-limited mass spectrum are observed. The ions at 15 and 105 amu correspond to the species observed after cleavage of the CH_3 group (Scheme 1a). The second pair at 77 and 43 amu corresponds to cleavage of the phenyl group (Scheme 1b). Finally, there is an ion at 92 amu, corresponding to toluene. The presence of toluene reveals that a strong-field dissociative rearrangement (compare with Fig. 1) of acetophenone is possible. The parent ion with a mass of 120 amu is not visible under these conditions but can be detected when lower intensity pulses are used. We probed whether we can control acetophenone's photochemistry by first optimizing the ratio $\text{C}_6\text{H}_5\text{CO}^+/\text{C}_6\text{H}_5^+$ (stipulating preferential cleavage of the methyl species rather than the phenyl species). The measured ratio is plotted as a function of generation in Fig. 5B.

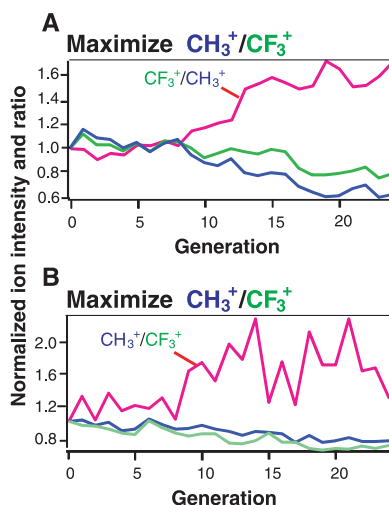


Fig. 4. A summary of competing reaction pathways for trifluoroacetone is shown. The average of the ratios (pink) of (A) $\text{CF}_3^+/\text{CH}_3^+$ and (B) $\text{CH}_3^+/\text{CF}_3^+$ is plotted as a function of generation. Also shown are the relative ion intensities for CH_3^+ (blue) and CF_3^+ (green). Maximization of the ratio is the specified goal of the algorithm, and extrema at any point in the learning curve represent the best yield [e.g., a maximum enhancement of ~ 2.2 is evident in (B)].

The enhancement in this case is a factor of 1.7. The phenylcarbonyl ion remains constant in intensity as the control algorithm progresses, whereas the phenyl ion is suppressed. The optimal pulse is not transform limited and is also complex (24). In these experiments, the $C_6H_5^+$ and $C_6H_5CO^+$ ions are in direct competition with each other when a given parent molecule is excited.

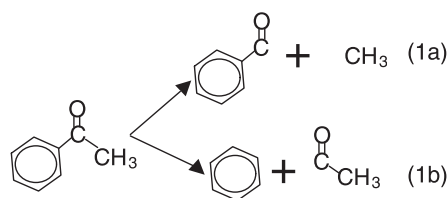
The second optimization goal imposed on the system was maximization of the opposite ratio, $C_6H_5^+/C_6H_5CO^+$, corresponding to preferential cleavage of the phenyl group. The learning curve for this process, Fig. 5C, again shows that the intensity of the phenylcarbonyl ion remains relatively constant, whereas the intensity of the phenyl ion increases. This is interesting because the energy required to cleave the phenyl-CO(CH₃) bond (100 kcal/mol) is ~15 kcal/mol higher than that for the methyl-CO(C₆H₅) bond (25). In both experiments, the algorithm enhanced the ratio by either increasing or decreasing the intensity of the phenyl ion while maintaining constant phenylcarbonyl intensity. We attribute the observed control to a nontrivial mechanism for several reasons. In the reference experiments (21), altering the intensity changed the $C_6H_5^+/C_6H_5CO^+$ ratio

with a dynamic range of 1.5, but this process required a change in $C_6H_5CO^+$ ion intensity of one order of magnitude. The tailored pulses in Fig. 5, B and C, exhibit a dynamic range of at least 4 in this ratio with no change in $C_6H_5CO^+$ ion intensity. Given the limited amount of amplitude and phase space explored by the experiment (e.g., tying 16 pixels together and the 6% mutation rate), it is likely that the optimal dynamic range from pulse tailoring is much larger. It is extremely unlikely that there are trivial intensity-pulse duration conditions that maintain constant phenylcarbonyl intensity while increasing or decreasing the phenyl intensity. In the reference experiments, we always found that the absolute ion intensity decreased monotonically with increasing pulse duration or decreasing pulse laser energy. Such correlation is not evident in the pulse-shaping experiments.

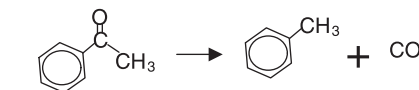
The goal of laser control of chemical reactivity transcends the simple unimolecular dissociation reactions observed to date (7, 8). Observation of the toluene ion in the strong-field acetophenone mass spectrum suggests that control of molecular dissociative rearrangement may be possible. To test this hypothesis, we specified the goal of maximizing the toluene yield from acetophenone, as shown in Scheme 2. For toluene to be produced from acetophenone, the loss of CO from the parent molecule must be accompanied by the formation of a bond between the

phenyl and methyl substituents. Conventional electron-impact mass spectrometric analysis of acetophenone revealed no evidence for toluene in the cracking pattern. The closed-loop control produced an increase in the ion yield at 92 amu of a factor of 4 as a function of generation, as shown in Fig. 5D. As a further test, we specified maximization of the ratio of toluene to phenyl ion and observed a similar learning curve to that in Fig. 5, B and C, with an enhancement in the toluene to phenyl ion ratio of a factor of 3. Again, the final tailored pulse does not resemble the transform-limited pulse (24). In order to confirm the identity of the toluene product, measurements on the deuterated acetophenone molecule $C_6H_5COCD_3$ were carried out, and the $C_6H_5CD_3^+$ ion was the observed product in an experiment analogous to that shown in Fig. 5D. The observation of optically driven dissociative rearrangement represents a new capability for strong-field chemistry. In such strong-field excitation, the electron dynamics during the pulse is known to be extreme, and substantial disturbance of the molecular eigenstates (compare with Fig. 2) can produce photochemical products, such as novel organic radicals, that are not evident in the weak-field excitation regime. Operating in the strong-field domain opens up the possibility of selectively attaining many new classes of photochemical reaction products.

Extensive manipulation of mass spectra is possible when shaped, strong-field laser pulses interact with molecules under closed-loop control. The control pulses occur with an intensity of $\sim 10^{13}$ W cm⁻², where the radiation substantially disturbs the field-free eigenstates of the molecule. Even in this highly nonlinear regime, the learning algorithm can identify pulse shapes that selectively cleave and rearrange organic functionality in polyatomic molecules. These collective results suggest that closed-loop strong-field laser control may have broad applicability in manipulating molecular reactivity. The relative ease in proceeding from one parent molecule to another should facilitate the rapid exploration of this capability.

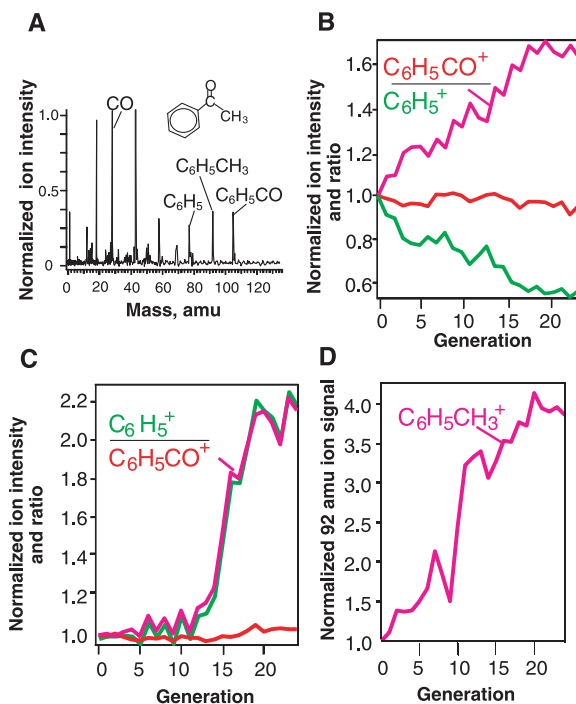


Scheme 1.



Scheme 2.

Fig. 5. (A) A transform-limited strong-field TOF mass spectrum for acetophenone. (B) The relative ion yield for phenylcarbonyl (red) and phenyl (green) and the $C_6H_5CO^+/C_6H_5^+$ ratio (pink) as a function of generation when maximization of this ratio is the specified goal in the closed-loop experiment. (C) The relative ion yield for phenylcarbonyl and phenyl and the $C_6H_5^+/C_6H_5CO^+$ ratio as a function of generation when maximization of this ratio is specified. (D) The average signal for toluene, 92 amu, as a function of generation when maximization of the ion signal for this reaction product was specified for optimization. Corresponding electron-impact ionization mass spectrometry revealed no evidence for toluene in the sample.



References and Notes

- R. S. Judson, H. Rabitz, *Phys. Rev. Lett.* **68**, 1500 (1992).
- C. J. Bardeen *et al.*, *Chem. Phys. Lett.* **280**, 151 (1997).
- T. C. Weinacht, J. L. White, P. H. Bucksbaum, *J. Phys. Chem. A* **103**, 10166 (1999).
- R. Bartels *et al.*, *Nature* **406**, 164 (2000).
- J. Kunde *et al.*, *Appl. Phys. Lett.* **77**, 924 (2000).
- F. Omenetto *et al.*, *Opt. Lett.*, in press.
- A. Assion *et al.*, *Science* **282**, 919 (1998).
- S. Vajda *et al.*, *Chem. Phys.*, in press.
- N. P. Moore, R. J. Levis, *J. Chem. Phys.* **112**, 1316 (2000).
- M. J. DeWitt, R. J. Levis, *Phys. Rev. Lett.* **81**, 5101 (1998).
- A. N. Markevitch, N. P. Moore, R. J. Levis, *Chem. Phys.*, in press.
- A. M. Weiner, *Prog. Quantum Electron.* **19**, 161 (1995).

13. H. Rabitz *et al.*, *Science* **288**, 824 (2000).
 14. H. Rabitz, W. S. Zhu, *Acc. Chem. Res.* **33**, 572 (2000).
 15. R. J. Levis, M. J. DeWitt, *J. Phys. Chem. A* **103**, 6493 (1999).
 16. J. M. Geremia, W. S. Zhu, H. Rabitz, *J. Chem. Phys.* **113**, 10841 (2000).
 17. M. M. Wefers, K. A. Nelson, *J. Opt. Soc. Am. B* **12**, 1343 (1995).
 18. D. Goldberg, *Genetic Algorithms in Search Optimization and Machine Learning* (Addison-Wesley, Reading, MA, 1989).
 19. M. Demiralp, H. Rabitz, *Phys. Rev. A* **47**, 809 (1993).
 20. K. Sundermann, H. Rabitz, R. de Vivie-Riedle, *Phys. Rev. A* **62**, 013409 (2000) (available at <http://link.aps.org/abstract/PRA/v62/e013409>).
 21. In the reference experiments, the intensity of the

laser pulse was decreased by inserting glass coverslips into the beam before focusing, which decreased the intensity by $\sim 7\%$ per slide. The pulse duration was increased by placing a linear chirp on the pulse by either increasing or decreasing the position of the second grating in the compressor. The mass spectra were recorded and analyzed as a function of these two variables to provide a reference for the shaped-pulse control experiments.
 22. M. J. DeWitt, R. J. Levis, *J. Chem. Phys.* **110**, 11368 (1999).
 23. R. J. Levis, G. M. Menkir, H. Rabitz, data not shown.
 24. Drawing unambiguous mechanistic conclusions from analysis of the detailed kinematic field structures alone is difficult at this time. Furthermore, before analyzing the field, suitable cost functions need to be

introduced in the algorithm guiding the experiments to assure that only the essential structure is retained (16).
 25. J. Berkowitz, G. B. Ellison, D. Gutman, *J. Chem. Phys.* **98**, 2744 (1994).
 26. The authors acknowledge the support of the Office of Naval Research, the Army Research Office, the NSF, and the Sloan and Dreyfus foundations for the support of this research. R.J.L. acknowledges fruitful discussions with A. Markevitch, N. P. Moore, and P. Graham.

18 January 2001; accepted 15 March 2001

Published online 29 March 2001;
 10.1126/science.1059133

Include this information when citing this paper.

A Complex Pattern of Mantle Flow in the Lau Backarc

Gideon P. Smith,¹ Douglas A. Wiens,¹ Karen M. Fischer,² Leroy M. Dorman,³ Spahr C. Webb,⁴ John A. Hildebrand³

Shear-wave splitting analysis of local events recorded on land and on the ocean floor in the Tonga arc and Lau backarc indicate a complex pattern of azimuthal anisotropy that cannot be explained by mantle flow coupled to the downgoing plate. These observations suggest that the direction of mantle flow rotates from convergence-parallel in the Fiji plateau to north-south beneath the Lau basin and arc-parallel beneath the Tonga arc. These results correlate with helium isotopes that map mantle flow of the Samoan plume into the Lau basin through an opening tear in the Pacific plate.

Seismic anisotropy (I) is usually attributed to the alignment of crystal orientations, which in turn can be related to the strain history of the rock (2–5). Strain can also be inferred from modeling of mantle flow (6), and thus observation of seismic anisotropy can be used to map mantle flow at length scales related to the wavelength of the seismic waves. Many observations of anisotropy have been made in the region of subduction zones (7). However, an unambiguous interpretation of these results is often difficult because of poor station coverage or nonuniform source distribution. Here we use a unique data set, which spans an active backarc basin and spreading center, to map out the mantle flow in a backarc system and compare the seismic measurements to geochemical studies and model predictions.

Modeling of the strain resulting from flow coupled to the subducting plate (6, 8) predicts a fairly uniform pattern of anisotropy, with a fast direction parallel to the absolute plate motion of the downgoing plate. A variety of shear-wave (S -wave) splitting measurements

at island stations in backarc areas are consistent with this pattern (9–14) or with flow coupled to both subducting and overlying plates. However, closer to the trench and slab, the pattern of mantle flow may become more complex. Large-scale deviation of mantle flow due to retrograde motion of the subducted slab has been postulated (15) and was reported by S -wave splitting studies in South America (16). Similar observations in New Zealand (17) and Kamchatka (18) may also result from such a flow pattern. Physical modeling of subduction zone flow also indicates strong variations in mineral alignment with slab dip (19). Numerical modeling of the likely induced lattice preferred orientation of olivine and orthopyroxene produces results that are non-unique and may only be fully tested with a more detailed mapping of the backarc system (13, 20). It is often difficult to infer the exact location of the anisotropy and thus to determine whether observations result from propagation within an anisotropic mantle wedge or within the slab.

In the Lau backarc, there is also the question of the effect of the small-scale processes associated with the spreading center. Although modeling predicts vertical preferential alignment of the olivine a axis due to the upwelling flow (21), a variety of fast directions have been noted in other spreading regions (22–26).

In this study, we present splitting mea-

surements from the Lau backarc. These observations provide strong constraints on lateral variations in the fast axis and thus allow us to distinguish geographic variations in anisotropy that may occur across the backarc basin. The region of the Lau basin and Tonga arc contains both an active backarc spreading center and a rapidly subducting slab (at a rate of 240 mm/year), so there should be a strong and variable signature of mantle flow. The high rate of seismic activity in this region also provides numerous high-energy sources for S -wave studies.

We analyzed S -wave splitting in arrivals from local earthquakes occurring beneath the Lau backarc. Data were obtained from the southwest Pacific seismic experiment (SPASE) and from the Lau basin ocean-bottom seismograph (OBS) survey (LaBatts). The SPASE array was deployed for 2 years and consisted of 12 broadband stations in Fiji, Tonga, and Niue Island. LaBatts was a concurrent 3-month deployment of 29 OBSs in the Lau backarc and Tonga forearc.

The OBS instrument orientations (27) were determined by comparing the polarization angles (28) of the P waves and Rayleigh waves from large, well-located, distant events, with known back azimuth. Splitting observations (29) were obtained using a cross-correlation of the two S waves calculated for a range of rotation angles, φ , and time offsets, δt (9). The δt and φ providing the maximum cross-correlation are the splitting time and fast anisotropy azimuth (Fig. 1). Some of the land station observations are taken from the analysis of Fischer and Wiens (10). Reanalysis of a subset of the Fischer and Wiens (10) data set using this method produced identical results, indicating that there is no bias between the results from the two studies. In order to avoid interference from the free surface or crustal phase conversions, we restricted our analysis to arrivals inside the S -wave “window” (incidence angles $< 35^\circ$).

Well-constrained splitting parameters were obtained for 77 arrivals at the OBS stations and were combined with the existing 53 observations at land stations (10). Seventeen new land observations were also obtained at Kadavu Island and at land stations at

¹Department of Earth and Planetary Sciences, Washington University in St. Louis, 1 Brookings Drive, CB1169, St. Louis, MO 63130, USA. ²Department of Geological Sciences, Box 1846, Brown University, Providence, RI 02912, USA. ³Scripps Institution of Oceanography, University of California, San Diego, La Jolla, CA 92093–0215, USA. ⁴Lamont-Doherty Earth Observatory, Post Office Box 1000, 61 Route 9W, Palisades, NY 10964, USA.